Sudan University of Science and Technology

College of Graduate Studies

كلية الدراسات العليا

A Theoretical Model of Er^{3+} –Yb^{3+} Using Downconversion Mechanism

نموذج نظري لـ Er^{3+} -Yb^{3+} باستخدام اليه التحويل الخافض

A Dissertation Submitted For Partial Fulfillment Requirements For The Degree Of M.S.C In Physics

Prepared by:

Ola Tarig Mustafa Alzebeer

Supervisor:

Dr. Mubarak Yagoub Adam

May /2018

DEDICATION

Every challenging work needs self-efforts as well as guidance of elders especially those who were very close to my heart.

My humble effort I dedicate to my father and mother whose affection, love, encouragement and prays to make me able to get such success and honor.

I dedicate this Dissertation to My husband Mohamed Awad Elkareem for his support.

ACKNOWLEDGEMENT

I would like to thank (ALLAH) for helping me and giving me life and time to accomplish this work. Thanks to Sudan University of Science and Technology for giving me the opportunity to present this work.

I extend my gratitude to my supervisor Dr. Mubarak Yagoub who gave me fruitful advice and support which has encouraged me throughout this whole process and for his guidance and supervision.

I would like to thanks everyone who have helped me with valuable advice and efforts.

Last but not least, I wish to thank my parents for being there, make me strong than I would be without them.

ABSTRACT

Solar energy is one of the most promising renewable energy sources. One of the major loss mechanisms leading to low energy conversion efficiencies of solar cells is the thermalization of charge carriers generated by the absorption of high-energy photons. These losses can largely be reduced by using downconversion mechanism. The purpose of this dissertation is the possibility of using Er^{3+} and Yb^{3+} as downconvertor. A theoretical rate equation model of the Er^{3+}-Yb^{3+} system are simulated numerically by using python in order to obtain the power conversion efficiency (PCE) and the quantum conversion efficiency (QCE).

المستخلص

الطاقة الشمسية واحدة من اهم مصادر الطاقة المتجددة , احد اسباب التى تؤدي الى محدودية كفاءة الخلية الشمسية هي التسخين الذي يحدث لحاملات الشحن المتولدة عن طريق امتصاص الفوتونات الضوئية ذات الطاقة العالية . هذا الفقد يمكن تقليله بصورة كبيرة عن طريق نظرية التحويل الخافض . يهدف هذا البحث الى امكانية استخدام Er^{3+} وYb^{3+} كخافضات تحويل يتم استخدام نموذج التحويل الخافض للعناصر Er^{3+} وYb^{3+} الذي تمت نمذجته عدديا باستخدام لغة بايسون للحصول على كفاءة الطاقة التحويلية وكفاءة الكم التحويلية للخلية الشمسية .

CONTENTS

Article	Page number
Dedication	I
Acknowledgement	II
Abstract	III
Abstract (Arabic)	IV
Contents	V
List of figures	VII
Chapter one Introduction	
1.1 General overview	1
1.2 Problem statement	2
1.3 Objectives	2
1.4 Thesis organization	2
Chapter two Background information	
2.1 Solar radiation	3
2.2 Solar cells	5
2.3 Spectral response	8
2.4 Solar cell conversion efficiency limits	10
2.5 Photon conversion processes	12
2.6 Lanthanide ions	14

2.7 Down-conversion mechanisms	17
2.7.1 Rate equation model of Er^{3+}-Yb^{3+} downconversion	19
Chapter three **Result**	
3.1Introduction	22
3.2 the theoretical model calculation	22
3.2.1 the effect Er^{3+}-Yb^{3+} concentration on PCE and QCE	24
3.2.2 the effect of the spectral down-converter thickness on PCE and QCE	26
Chapter four **Discussion and conclusion**	
4.1 Discussion	28
4.2 Conclusions	28
References	29

LIST OF FIGURES

Figures	Page number
Fig.2.1 The global spectral solar spectrum on the earth for air mass	3
Fig.2.2 Schematic diagram showing the calculation of the air mass (AM).	4
Fig.2.3 Behaviour of light shining on a solar cell	6
Fig.2.4 The ideal short circuit flow of electrons and holes at a *p-n* junction	7
Possible modes of recombination of electron-hole pairs	7
Fig.2.6 The effect of light on the current-voltage characteristics of a *p-n* junction	7
Fig.2.7 The creation of electron-hole pairs and dissipation of energy in excess Of *Eg*	8
Fig.2.8 Bandgap limitations on the quantum efficiency of silicon solar cells	9
Fig.2.9 The quantum limit of spectral responsivity as a function of wavelength	9
Fig.2.10 Schematic diagram showing the Photon luminescence conversion processes	12
Fig.2.11 Spectral conversion design for PV applications	13
Fig.2.12 Free ion energy levels of the trivalent lanthanide ions(dieke diagram)	16
Fig.2.13 schematic diagram of typical mechanisms of NIR quantum cutting	18
Fig.2.14 Energy level scheme of the Er^{3+} and Yb^{3+}	19
Fig.3.1 the thickness of the spectral down-converter and variation of PCE and QCE with Er^{3+} and Yb^{3+}	25
Fig.3.2 $Er^{3+}$and Yb^{3+} concentration and variation of PCE and QCE with the thickness	27

CHAPTER ONE

INTRODUCTION

1.1 General Overview

Renewable resources are clean or green energy sources that give much lower environmental impact than conventional energy sources .Renewable resources are attractive because they are replenished naturally, which means that they will never run out. Solar cells one of renewable resources. Solar cell is an electrical device that converts the energy of light directly into electricity. Shockley–Queisser limit state that the maximum theoretical efficiency of a solar cell using a single p-n junction to collect power from the cell is around 30 % [1]. To improve the efficiency an interesting technique has been proposed to convert incident high energy photons into either an equal number or more of photons of smaller energy before absorption in the solar cell [2]. In this way, the number of high energy photons absorbed in the cell decreases, without the total number of absorbed photons decreasing. Consequently, the number of hot charge carriers generated by these photons decreases too, and the available energy lost by thermalization of the hot charge carriers is diminished. The authors stated that this technique may increase the solar cell efficiency incident non-concentrated radiation is considered. Two processes have been mainly studied since the original work [2] was published. They were called down-conversion and up-conversion, in the first process, which is sometimes referred to as quantum-cutting via down-conversion [3], more than one low energy photon is produced from absorption of one high energy photon. In the second process two low energy infrared photons that cannot be absorbed by the solar cell, are added up to give one high energy photon that can be absorbed, the main energy loss in the conversion of solar energy to electricity is related to the spectral mismatch. We use lanthanide ions for spectral conversion in solar cells for rich and unique energy level structure arising from the $4f^n$ inner shell configuration of the

trivalent lanthanide ions gives a variety of options for efficient and down-conversion.

1.2 Problem Statement

The way to reduce the energy losses in a semiconductor solar cell is the generation of multiple electron–hole pairs per incident photon for photon energies larger than twice the band-gap energy of the solar cell material. In this work the possibility of using the lanthanide ions of Er^{3+} and Yb^{3+} downconversion mechanism to overcome this problem is proposed.

1.3 Objectives

This work aimed mainly to:

- Get more information about down-conversion.
- Know the relation between lanthanide ions and solar cell.
- The possibility to improve the efficiency of the solar cell using lanthanide ions based material.
- Using rate equation for modelling the downconversion layer.

1.4 Dissertation Organization

This dissertation consist of four chapters. In chapter one, a general introduction, problem statement and objective were given. Background information on solar cell and downconversion system where discussed in chapter two. Chapter three show the results generated by using rate equations method for modelling the downconversion. Discussion and future works were represented in chapter four.

CHAPTER TWO

BACKGROUND INFORMATION

2.0 INTRODUCTION

In this chapter the basic concepts that are necessary to understand the theory of this study are reviewed and explained.

2.1 Solar Radiation

The sun emits a nearly continuous spectrum ranging from ultraviolet, visible and infrared parts of electromagnetic radiation. The distribution of electromagnetic radiation as a function of wavelength is called the solar spectrum or solar radiation. Fig.2.1 shows the solar irradiance as a function of wavelength (λ) at a point outside the earth's atmosphere.

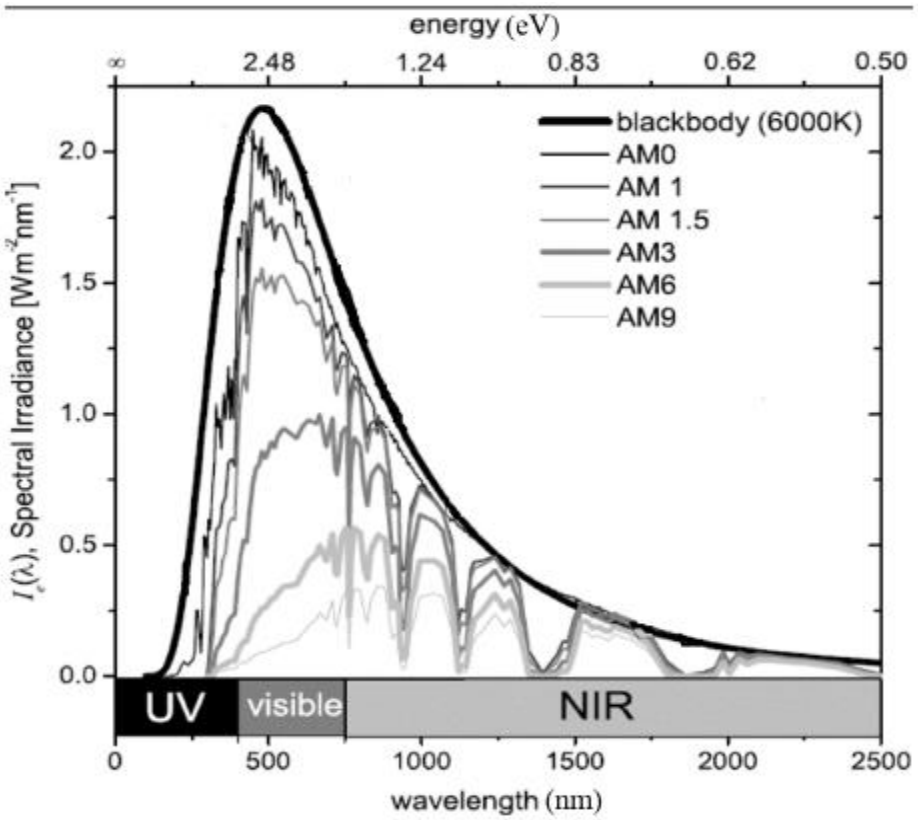

Fig. 2.1: The global spectral solar spectrum on the earth for air mass (AM) = 0 to 9. It can be seen that the AM0 spectra closely matches that for a black-body radiation. Adopted from A [4].

At a point just outside the sun surface, the total intensity value is1376 W m^2. This corresponds to the air mass zero (AM0) solar spectrum and is used for calibration of solar cell performance in space. The AM measures the path length of radiation relative to the length of the direct beam path through the atmosphere and is given by 1/cos(θ) see (Fig.2.2). The AM0 value rapidly decreases when the sun light passes through the earth's atmosphere or with increasing the air mass (AM). The journey of the solar radiation through the earth's atmosphere causes the attenuation of the solar radiation due to the scattering and absorption by atmospheric gases [4]. Fig.2.1 shows the influence of the earth's atmosphere on the solar radiation with increasing AM values.

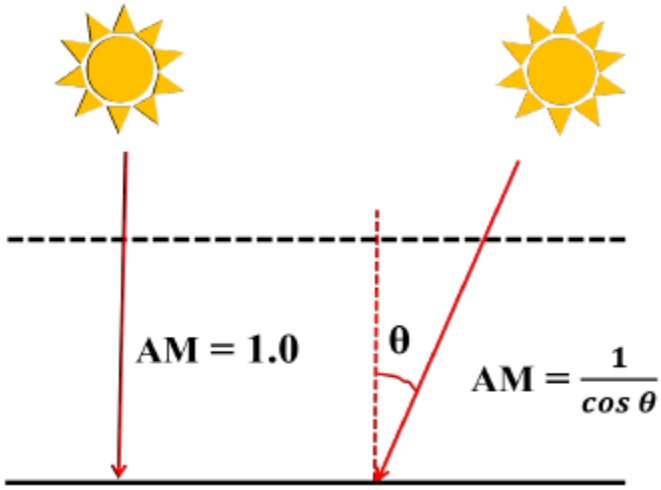

Fig. 2.2: Schematic diagram showing the calculation of the air mass (AM).

The standard solar spectrum for temperature latitude is AM1.5 corresponding to θ = 48.2°. The terrestrial solar spectrum has been normalized so that the integrated irradiance is 1000 Wm^{-2}. Actual irradiances clearly differ with account to seasonal and daily variations in the position of the sun, orientation of the earth and condition of the sky [5].

2.2 Solar Cells

A solar cell or photovoltaic cell is an electrical device that converts the energy of light directly into electricity by the photovoltaic effect, which is a physical and chemical phenomenon. It is a form of photoelectric cell, defined as a device whose electrical characteristics, such as current, voltage, or resistance, vary when exposed to light. Solar cells are the building blocks of photovoltaic modules, otherwise known as solar panels.

Solar cells are described as being photovoltaic, irrespective of whether the source is sunlight or an artificial light. They are used as a photo detector (detecting light or other electromagnetic radiation near the visible range), or measuring light intensity [2].

The operation of a photovoltaic (PV) cell requires three basic attributes:

- The absorption of light, generating electron-hole pairs.
- The separation of charge carriers of opposite types.
- The separate extraction of those carriers to an external circuit.

A silicon solar cell is a diode formed by joining p-type (typically boron doped) and n-type (Typically phosphorous doped) silicon. Light shining on such a cell can behave in a number of ways, as illustrated in Fig. 2.3. To maximize the power rating of a solar cell, it must be designed so as to maximize desired absorption (3) and absorption after reflection (5).

The electric field $\hat{E}$ at the p-n junction sweeps electrons to the n side and holes to the p side. The ideal flow at short circuit is shown in Fig. 2.4. However, some electron hole (e-h) pairs get lost before collection, as shown in Fig.2.5.

In general, the closer the point of e-h generation to the p-n junction, the better the chance of collection. Collected carriers are those that generate a finite current when V = 0. Chances of collection are particularly good if the e-h pairs are generated within a diffusion length of the junction. The light has the effect of shifting the I-V curve down into the fourth quadrant where power can be

extracted from the diode. I-V curve characterizes the cell, with its power output being equal to the area of the rectangle in the bottom right-hand quadrant of Fig. 2.6 [6].

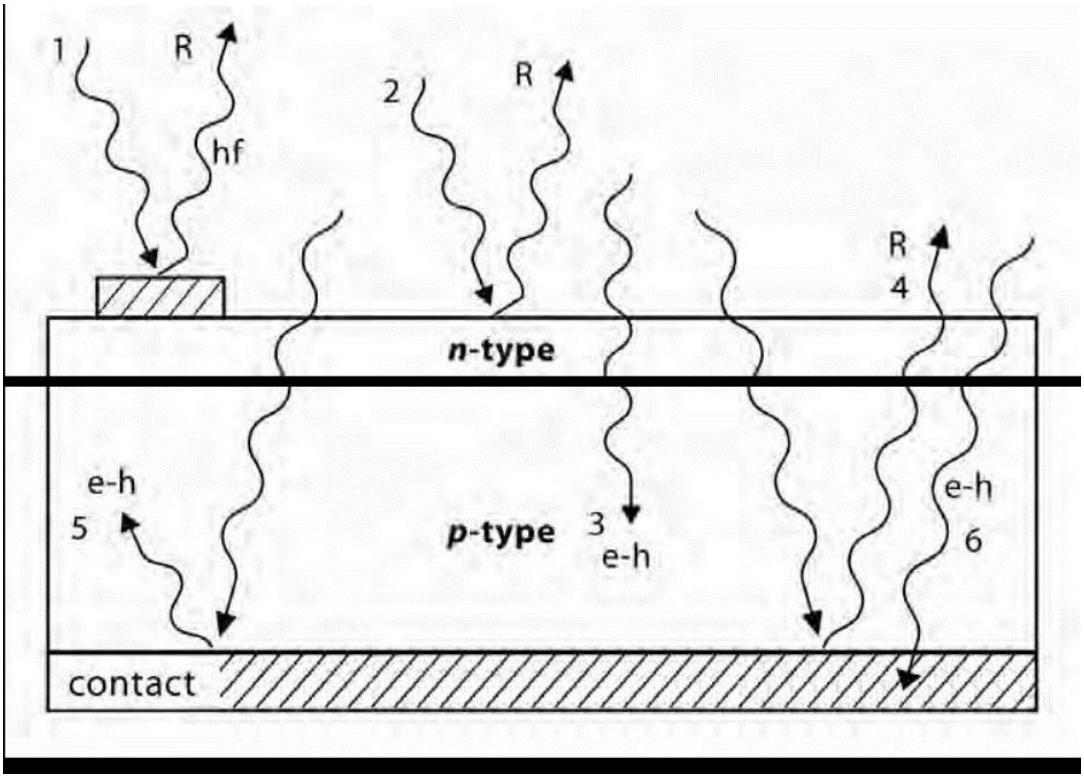

Fig.2.3: Behaviour of light shining on a solar cell. (1) Reflection and absorption at top contact. (2) Reflection at cell surface. (3) Desired absorption. (4) Reflection from rear out of cell—weakly absorbed light only. (5) Absorption after reflection. (6) Absorption in rear contact [6].

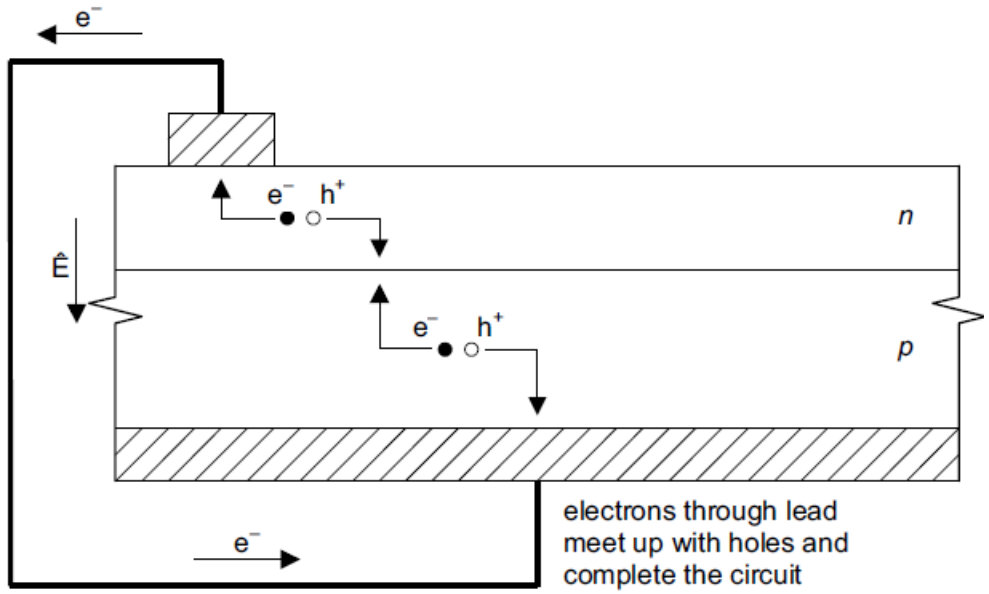

Fig.2.4: The ideal short circuit flow of electrons and holes at a *p*-*n* junction [6].

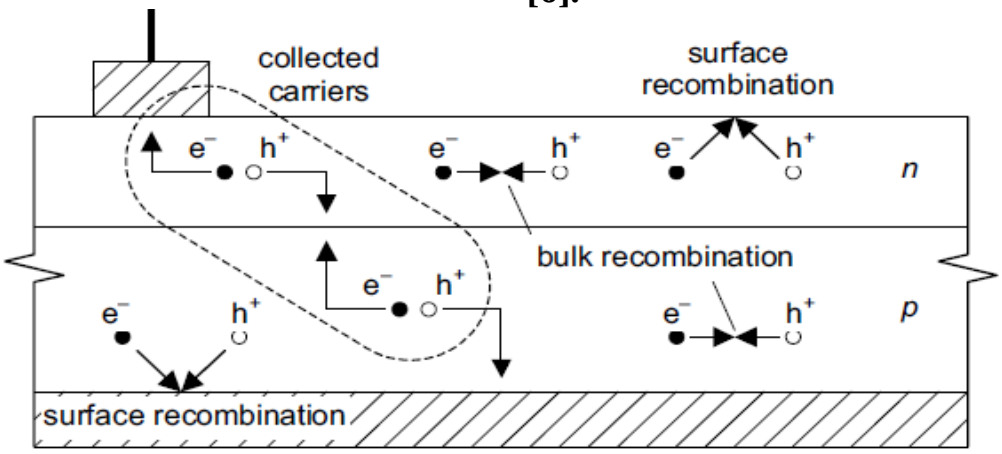

Fig.2.5: Possible modes of recombination of electron-hole pairs, showing collection of carriers that do not recombine [6].

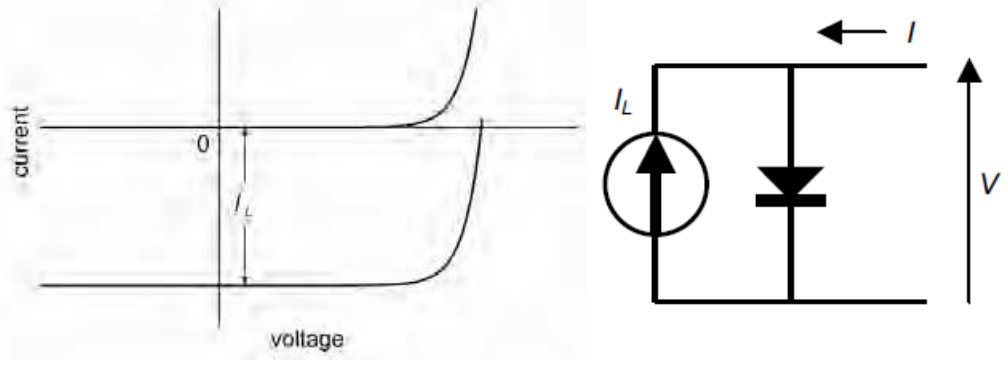

(a) **(b)**

Fig.2.6: The effect of light on the current-voltage characteristics of a *p*-*n* junction [6].

2.3 Spectral Response

Solar cells respond to individual photons of incident light by absorbing them to produce an electron-hole pair, provided the photon energy (E_{ph}) is greater than the bandgap energy (E_g). Photon energy in excess of E_g is quickly dissipated as heat, as shown in Fig.2.7.

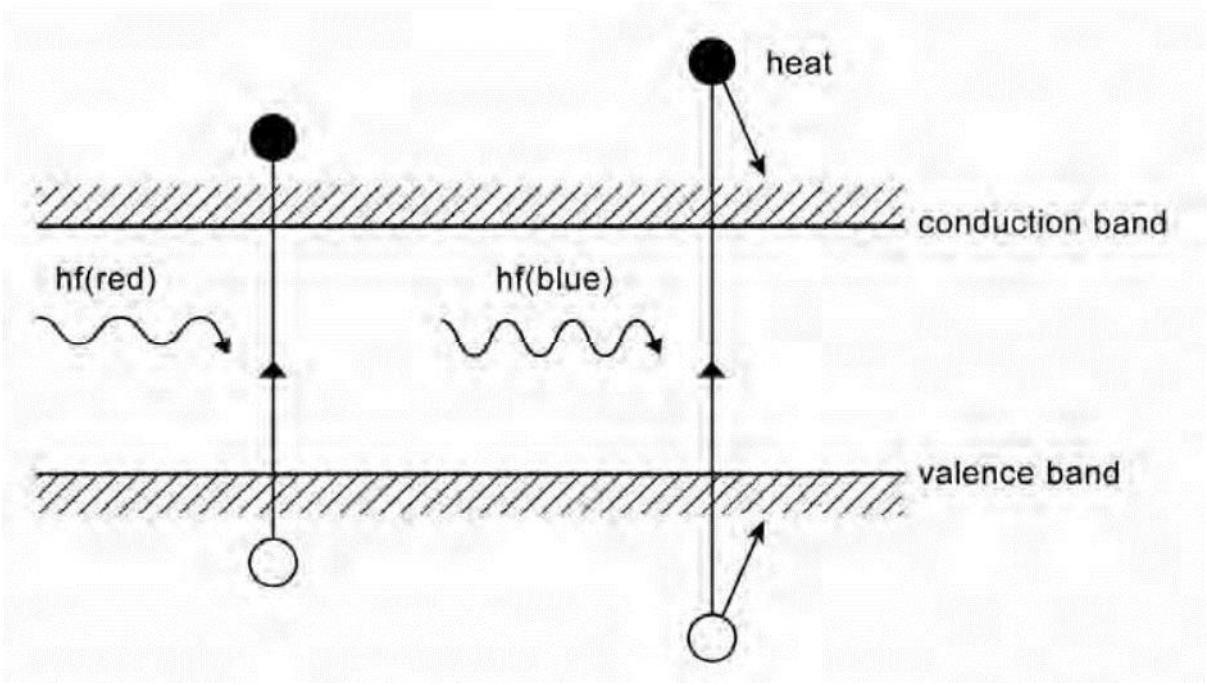

Fig.2.7. the creation of electron-hole pairs and dissipation of energy in excess of *Eg* [6].

The quantum efficiency (QE) of a solar cell is defined as the number of electrons moving from the valence band to the conduction band per incident photon. The longest wavelength for which this is finite is limited by its bandgap. Maximum use can only be made of incoming sunlight if the bandgap is in the range 1.0–1.6 eV. This effect alone acts to limit the maximum achievable efficiency of solar cells to 44% [5]. The bandgap of silicon, at 1.1 eV, is close to optimum, while that of gallium arsenide, at 1.4 eV, and is even better, in principle. Fig. 2.8 illustrates the dependence of ideal quantum efficiency on bandgap. Also of interest is the spectral responsivity of a solar cell, given by the amperes generated per watt of incident light (Fig. 2.9). Ideally, this increases with wavelength. However, at short wavelengths, cells

cannot use all the energy in the photons, whereas at long wavelengths, the weak absorption of light means that most photons are absorbed along the way from the collecting junction and the finite diffusion length in the cell material limits the cell's response.

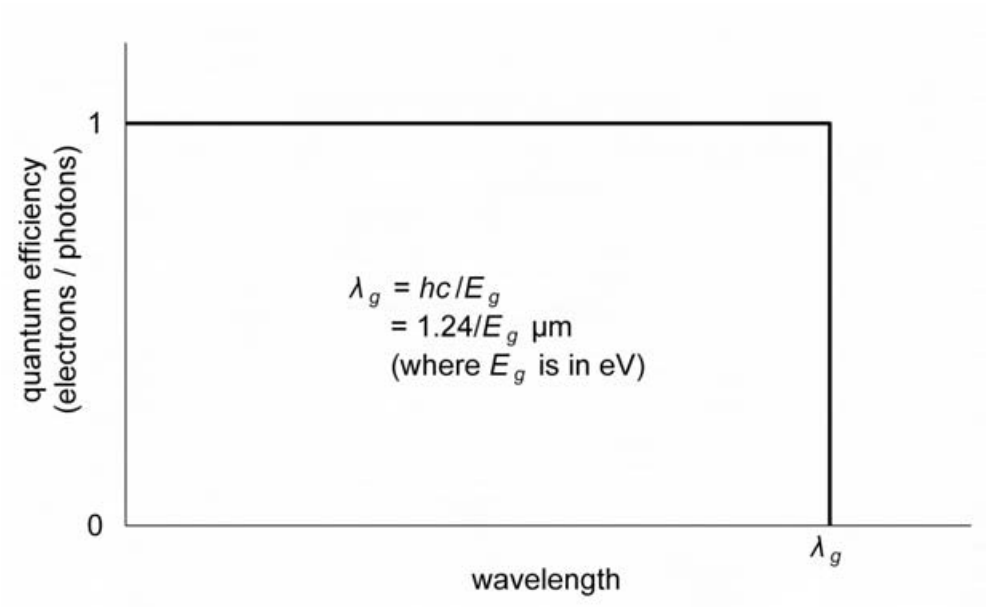

Figure 2.8: Bandgap limitations on the quantum efficiency of silicon solar cells [6].

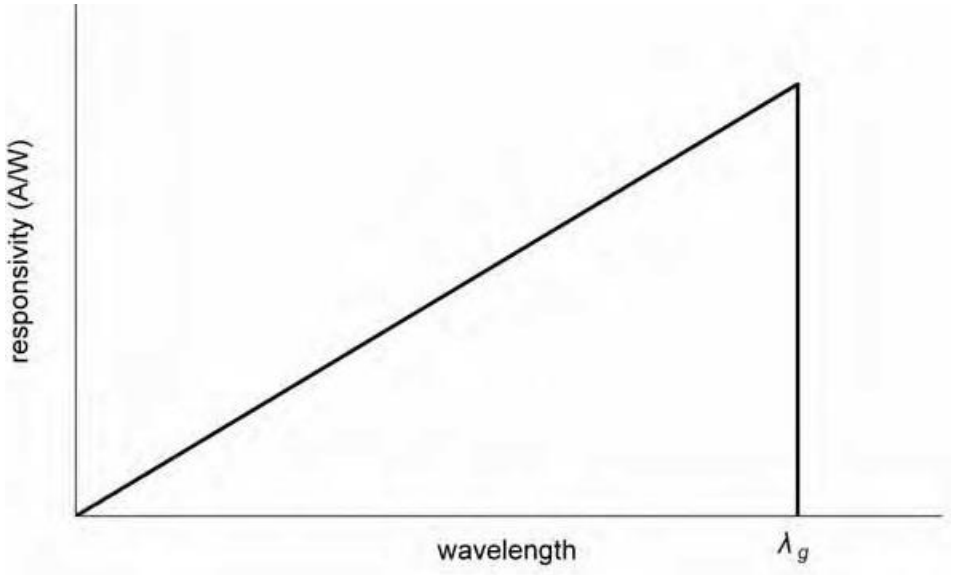

Fig2.9: The quantum limit of spectral responsivity as a function of wavelength [6].

2.4 Solar Cell Conversion Efficiency Limits

The maximum conversion efficiency (η) of a solar cell is defined as the ratio of maximum power (P_m) generated by a solar cell to incident power (P_{in}). The incident power normally equal to the AM1.5 irradiance spectrum, which is also equal to the total optical density (power per unit area) incident on the solar cell. Pm is defined as the voltage at maximum power point (V_m) multiplied by the maximum current density at that point [3, 5].

$$\eta = \frac{P_m}{p_{in}} = \frac{J_m V_m}{P_{in}} = \frac{J_{sc} V_{oc} FF}{P_{in}} \qquad (2.1)$$

Where J_{sc} and V_{oc} are the short-circuit current density and open circuit voltage, respectively. FF is the fill factor describing the `squareness' of the IV curve. Low band-gap materials have high thermalization losses (giving low V_{oc} and V_m), whereas high bandgap materials have low J_m and J_{sc} due to their maximum sub-bandgap losses [3]. The incident power can be calculated from the spectral power density, P (λ), using the following equation.

$$P_{in} = \int_0^\infty \frac{\varphi(\lambda) hc}{\lambda} d\lambda \qquad (2.2)$$

Where φ(λ) is the photon flux density and P(λ) = $\frac{\varphi(\lambda) hc}{\lambda}$. c is the speed of light and h is Plank's constant.

In principle, only photons with energy higher than the semiconductor energy bandgap (E_G) are utilized to generated e-h pairs. The fraction of incident energy that is absorbed by the single junction solar cell and used in energy conversion is given by:-

$$P_{abs} = \frac{\int_0^{\lambda_G} \frac{\varphi(\lambda) hc}{\lambda} d\lambda}{\int_0^{\infty} \frac{\varphi(\lambda) hc}{\lambda} d\lambda} \qquad (2\text{-}3)$$

Where λ_G is the wavelength of photons that corresponds to the energy bandgap of the absorber of the solar cell. A part of the absorbed energy, the excess photon energy, is lost due to the thermalization of electrons and holes to the edge of the conduction and valance bands of the absorber material. The fraction

of the absorbed energy that the solar cell utilized as useful energy, P_{use}, is given by

$$P_{use} = \frac{E_G \int_0^{\lambda_G} \varphi(\lambda) d\lambda}{\int_0^{\infty} \frac{\varphi(\lambda) hc}{\lambda} d\lambda} \qquad (2\text{-}4)$$

Therefore, we can write the conversion efficiency limited by the spectral mismatch as [3]

$$\eta = P_{abs} \times P_{use} = \frac{\int_0^{\lambda_G} \frac{\varphi(\lambda) hc}{\lambda} d\lambda}{\int_0^{\infty} \frac{\varphi(\lambda) hc}{\lambda} d\lambda} \frac{E_G \int_0^{\lambda_G} \varphi(\lambda) d\lambda}{\int_0^{\infty} \frac{\varphi(\lambda) hc}{\lambda} d\lambda} \qquad (2\text{-}5)$$

This equation consists of the transmission loss and the thermalization loss. These losses are known as spectral mismatch losses [3]. The thermalization loss is dominate in solar cells with small band-gap solar cell materials, whereas the transmission loss is substantial in semiconductors with wider band-gap and it occurs to the photons with energy smaller than the band-gap of silicon. According to the detailed balance model developed by Shockley and Queisser [1], the theoretical conversion efficiency limit for a single-junction solar cell with energy gap 1.1 eV is 30%. The spectral mismatch losses account for 70% of the total conversion efficiency limit [7]. Hence, proposals are needed to raise the existing solar cells beyond the Shockley-Queisser limit. One approach theory was developed to adapt the solar spectrum to better be used by the solar cells. This is to convert the high and low photons energy (thermalization and transmission losses) to where the spectral response of the solar cells is high using the concept of photon conversion processes. The basic concepts of the photon conversion processes will be discussed in the next section.

2.5 Photon Conversion Processes

Photon conversion processes aim to adapt the solar spectrum to better match the absorption properties of the solar cell device via luminescence. This is in contrast to the other concepts which all concern to develop a semiconductor device to better match the solar spectrum such as space-separated quantum cutting and multiple exciton generation [8]. There are three photon conversion processes, namely, down-shifting, down-conversion and up-conversion. These processes are illustrated schematically in Fig.2.10.

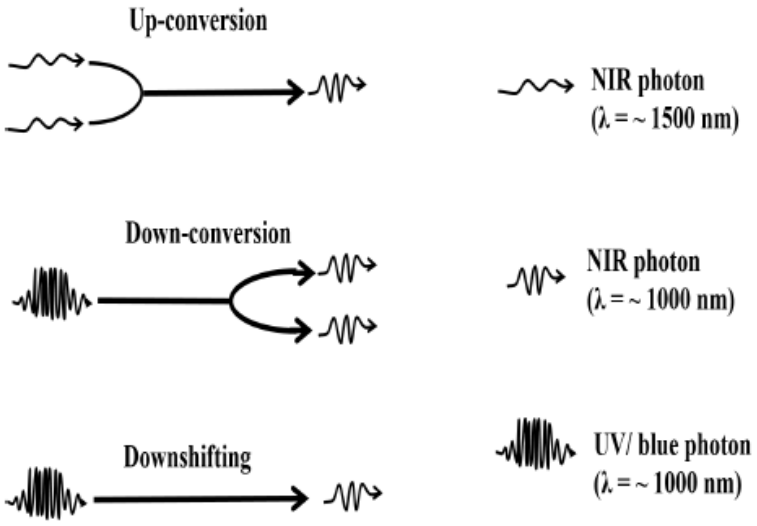

Fig. 2.10: Schematic diagram showing the photon luminescence conversion processes.

Up-conversion is where two lower energy photons combine to give one higher energy photon. The sum of the absorbed photons energies must be greater or equal to the emitted photons energies. Up-conversion is an anti-Stokes shifts since Stokes law states that the wavelength of the emitted light should be greater than the wavelength of the exciting spectrum. For solar cell application, a un-converter material could be placed behind a bifacial solar cell to convert the sub band-gap photons to higher energy photons back to the solar cell where they can be absorbed (Fig.2.11). The up-conversion processes can occur through three different mechanisms, namely excited state absorption, direct two photon absorption, and energy transfer up-conversion [9]. A detailed description

of the up-conversion process and its history can be found elsewhere [9]. Down-conversion is where one high energy photon (i.e. UV/visible photon) splits into two low energy photons. Whereas, downshifting is a process of shifting one higher energy photon into one lower energy photon. Both down-conversion and downshifting layers should be placed on top of a bificial single-junction solar cell to convert the high energy photons to lower energy photons where the spectral response of the solar cell is high and hence minimize the thermalization loss (Fig.2.11).

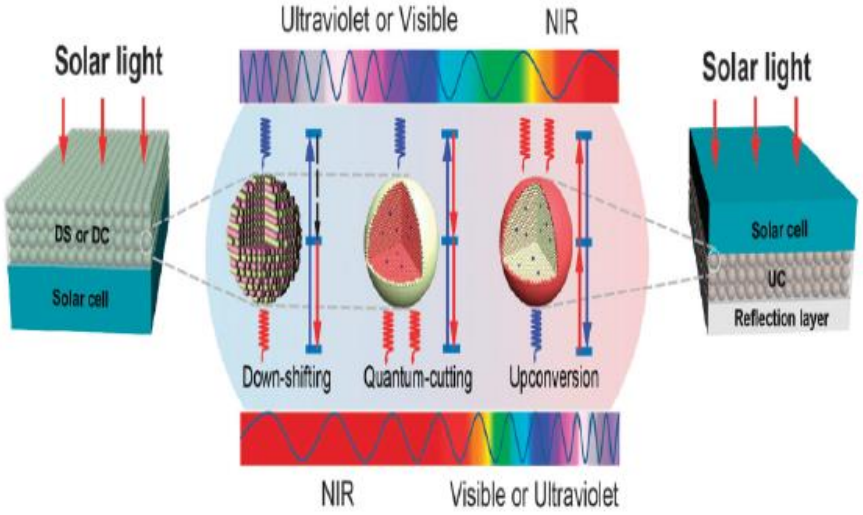

Fig. 2.11: Spectral conversion design for PV applications including downshifting (Ds), down-conversion (DC) and up-conversion (UP) luminescent materials [10].

Luminescent materials provide the most vital options for photon conversion processes. This project focused on the possibility of using lanthanide ions to enhance the spectral response of luminescent materials based on down-conversion, which will be therefore further discussed in the next sections.

2.6 Lanthanide Ions

The lanthanides are a group of elements found at the bottom of the periodic table. It is the series of elements where the 4f inner shell is not filled with electrons. They are mostly stable in the trivalent form and the Ln^{3+} -ions have the electronic configuration [Xe] $4f^n\ 5s^2\ 5p^6$ where n varies from 0 to 14. The partly filled 4f inner shell is responsible for the characteristic optical (and also magnetic) properties of the lanthanides. The number of configurations for n electrons divided over the fourteen 4f orbitals is large$\binom{14}{n}$. All configurations can have different energies, giving rise to energy levels in the UV, visible and (near) infra-red part of the spectrum. For the free ion, the energy levels are labelled by so-called term symbols ($^{2s+1}L_J$) [11]. Fig. 2.12 shows the energy level structure of the $4f^n$ configuration of the trivalent lanthanide ions. This diagram, often referred to as the Dieke diagram (In recognition of Gerard H. Dieke who originally published the diagram) [12, 13]. Clearly exhibits the rich energy level structure of these ions. This energy level diagram is also representative of the 4f energy level structure of these ions when doped into various kinds of crystalline or glassy materials. This is due to the optically active 4f orbital being well-shielded from the host environment by the outer filled 5s and 5p orbitals [11]. Still, the surrounding crystal field induces small Stark splitting of the energy levels, typically of the order of $\sim 10^2$ cm^{-1}. Phonons in the host material mediate non-radiative relaxation between excited energy levels. The peculiar optical properties of the lanthanides were first studied by Becquerel in the beginning of the 20^{th} century. He observed sharp absorption lines for lanthanide salts at low temperature. This observation was explained by Becquerel, Bethe and Kramers: the absorption lines originate from 4f intra-configurational transitions. Since the 4f electrons do not participate in bonding, absorption (and emission) lines will be very sharp. According to selection rules intra-configurational transitions, such as the 4f-4f transitions of the lanthanides,

are not allowed as electric dipole transitions since the initial and final state have the same parity. Mixing of opposite parity states into the 4f states partly lifts the selection rule, explaining the observed intensities of the 4f-4f transitions.

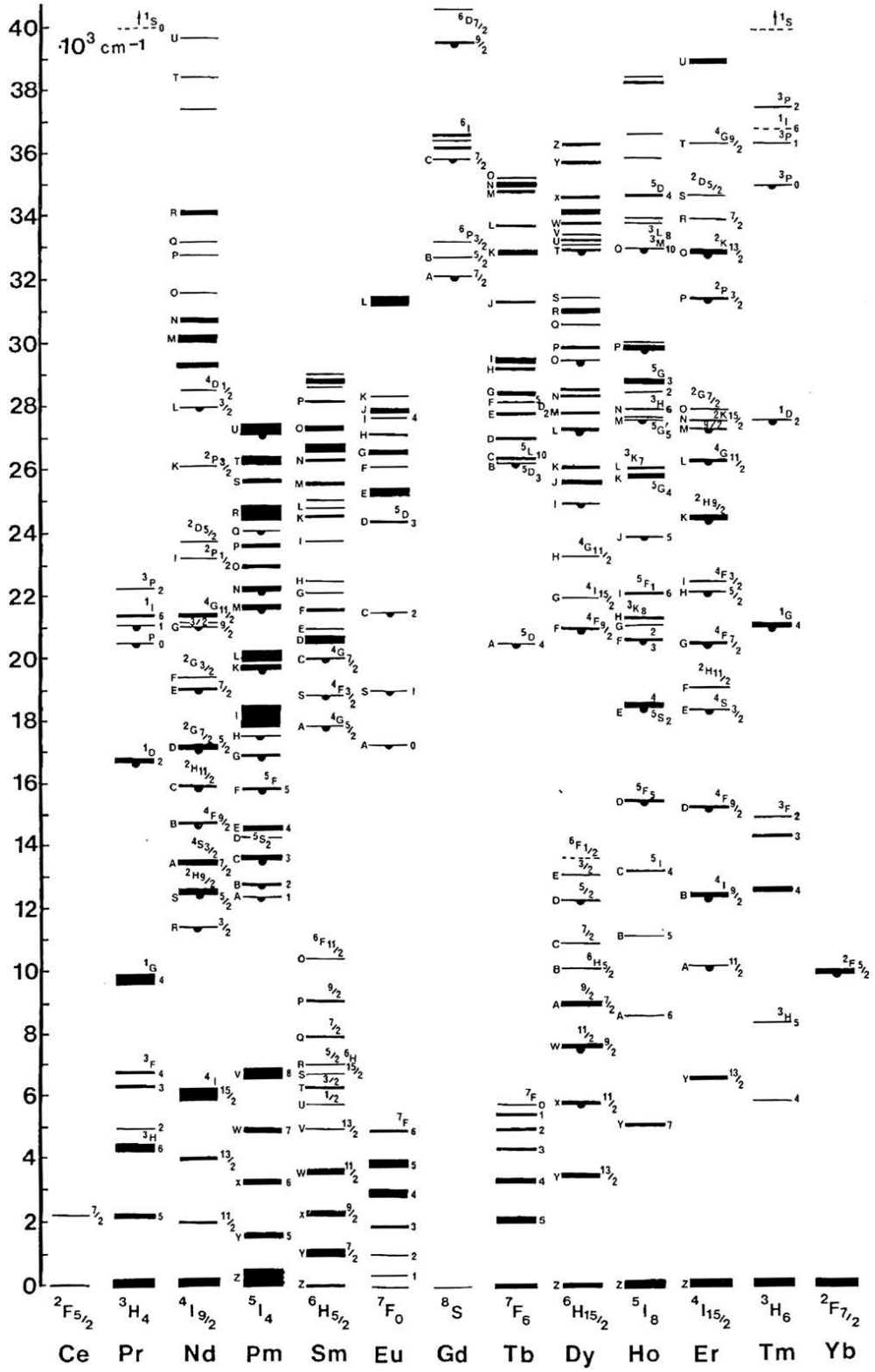

Figure 2.12: Free ion energy levels of the trivalent lanthanide ions from Ce^{3+} ($4f^1$) to Yb^{3+} ($4f^{13}$). Levels are labelled by term symbols or for some higher levels capital letters [12].

2.7 Down-Conversion Mechanisms

An interesting technique has been proposed by Trupke et al. [2] in 1957 to convert incident high energy photons into either an equal number or more of photons of smaller energy before absorption in the solar cell. In this way, the number of high energy photons absorbed in the cell decreases, without the total number of absorbed photons decreasing. Consequently, the number of hot charge carriers Generated by these photons decreases too and the available energy lost by thermalization of the hot charge carriers is diminished.

The idea to obtain quantum yields above 100% by creating multiple photons through 'cutting' a single photon into two lower energy photons. The mechanism involved the simultaneous energy transfer from a donor to two acceptors, each accepting half the energy of the excited donor. The aim was to achieve the emission of two visible photons from a single UV photon in order to boost the efficiency of light emitting devices (such as fluorescent tubes). The potential of down conversion for increasing the efficiency of solar cells was realized soon afterwards [7]. A theory has predicted that by using a down-conversion layer in conjunction with a Si solar cell, an energy efficiency of 38.6% can be achieved [7].

Different mechanisms that demonstrate the NIR quantum cutting are shown in Fig.2.13. Quantum cutting can occur with only one optically active center ion or with a combination of different ion centers. The single quantum cutting process consists of one ion with more than two energy levels. Excitation into the highest excited state yields two photon due to relaxation stepwise to the ground state, shown in Fig.2.13 (a). This was demonstrated in Er^{3+} and Ho^{3+} where upon absorption UV/V photon yields two NIR photons [14]. However, a major problem of using single ion based quantum cutting is the recombination of both unwanted UV/V and non-radiative emissions that compete with the desired emission of the two NIR photons [12].

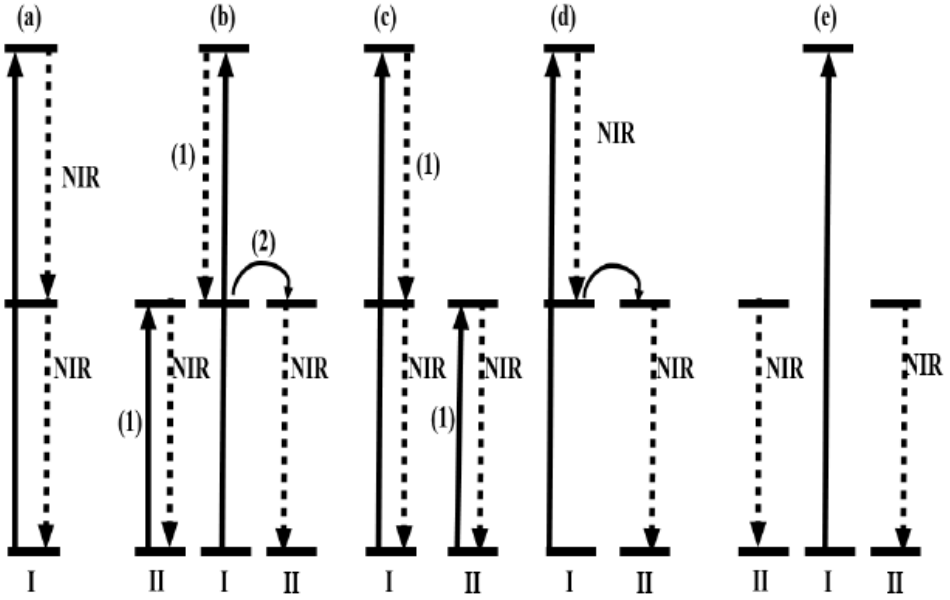

Fig. 2.13: Schematic diagram of typical mechanisms of NIR quantum cutting. (a) NIR quantum cutting on a single ion by the sequential emission of two NIR photons. (b-d)NIR quantum cutting due to resonant energy transfer from donor to an acceptor. (e)NIR quantum cutting due to cooperative energy transfer.

Another possibility is that quantum cutting occurs within more than one ion (are summarized in Fig.2.13 (b-e)) through cross-relaxation or resonant energy transfer between the ions. The energy resonance condition needs to be fulfilled. Quantum cutting can also occur by the use of three optically active centers. Fig. 2.13(b) shows the emission of two photons from ion pairs via cross-relaxation between the donor and acceptor ions followed by emission from the acceptor ions. There are some cases where quantum cutting may occur through cooperative energy transfer where the emission of the donor ion simultaneously excite two nearby ions through a cooperative process. The energy resonance had to be fulfilled, the energy difference for the energy transfer transitions in both ions have to be equal.

The energy transfer process in quantum cutting system can be investigated by the steady-state and time-resolved luminescence spectroscopy [15]. The energy

transfer (η_{ET}) and quantum efficiency (η_{QE}) is usually calculated from the luminescence decay curves using the following equations

$$\eta_{ET} = \eta_x \%acc = 1 - \frac{\int Ix\%acc\ dt}{\int I0\%acc\ dt} \qquad (2\text{-}6)$$

$$\eta_{QE} = \eta_{Don}(1- \eta_{ET}) + 2\eta_{ET} \qquad (2\text{-}7)$$

Where I represents the intensity and x%Acc stands for the acceptor concentration, and η_{Don} represents the quantum efficiency for the donor and is set to 1. The relative quantum efficiency was also determined through careful comparison of integrated areas from the emission spectra [16].

2.7.1 Rate equation model of Er^{3+}-Yb^{3+} downconversion

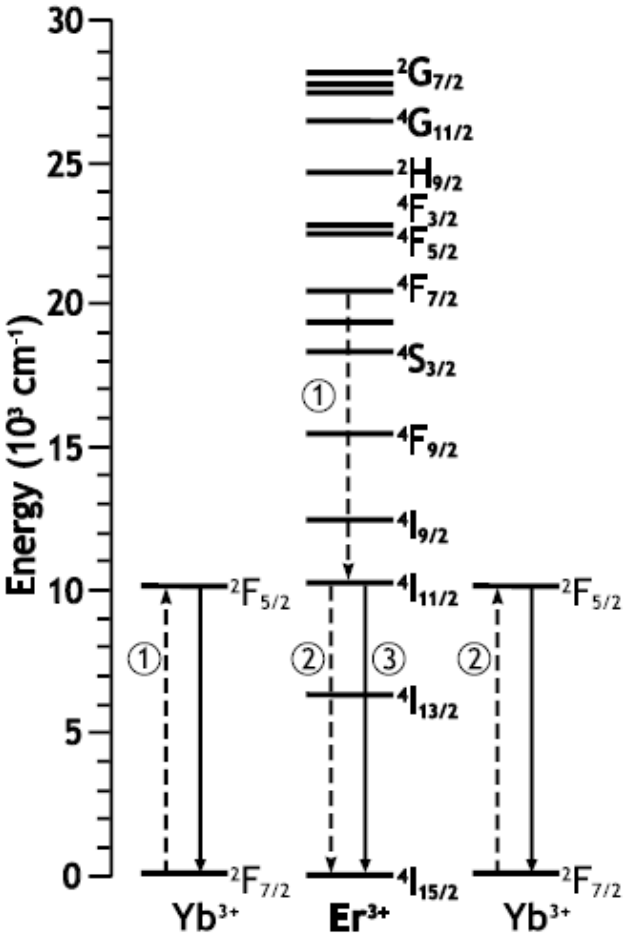

Fig.2.14: Energy level scheme of the Er^{3+} ($4f^{11}$) and Yb^{3+} ($4f^{13}$) couple showing two possible mechanisms for downconversion.

The diagram of Er^{3+} and Yb^{3+} energy levels, the relevant absorption and emission transitions, spontaneous emission, and the energy transfer process between Er^{3+} and Yb^{3+} is shown in Fig.2.14 Er^{3+} ion, when excited by blue photons into the $^4F_{7/2}$, relax nonradiatively to the $^4I_{7/2}$ level and then can interact with Yb^{3+} ions through a two-step consecutive energy transfer (ET). The QC processes are depicted schematically: Resonant ET transfers from the level of the Er^{3+} donor, and sequential transferred to two neighbouring Yb^{3+} acceptors, $Er^{3+}(^4F_{7/2})+Yb^{3+}(^2F_{7/2})\rightarrow Er^{3+}(^4I_{11/2})+Yb^{3+}(2F_{5/2})$ and $Er^{3+}(^4I_{11/2}) + Yb^{3+}(^2F_{7/2}) \rightarrow Er^{3+}(^4I_{15/2}) + Yb^{3+}(^2F_{5/2})$. Referring to the energy level system of Er^{3+}-Yb^{3+} as high lighted in Fig. 3.1, the QC system of Er^{3+}-Yb^{3+} is equivalent to a system of pump, excitation and transition. We propose the population-rate and power propagation equations model of Er^{3+}-Yb^{3+}. The group of rate and power propagation equations can be written as follows:

$$\partial N_1/\partial t = -W_{13} N1 + W_{21}N_2 + A_{21}N_2 + Ccr_2N_2N_5 \quad (2\text{-}8)$$

$$\partial N_2/\partial t = W_{32}N_3 + A_{32}N_3 - W_{21}N_2 - A_{21}N_2 + Ccr_1N_3N_5 - Ccr_2N_2N_5 \quad (2\text{-}9)$$

$$\partial N_3/\partial t = W_{13}N_1 - A_{32}N_3 \quad (2\text{-}10)$$

$$\partial N_4/\partial t = - W_{45}N_4 + W_{54}N_5 + A_{54}N_5 - Ccr_1N_3N_5 - Ccr_2N_2N_5 \quad (2\text{-}11)$$

$$\partial N_5/\partial t = -W_{54}N_5 + W_{45}N_4 - A_{54}N6 + Ccr_1N_3N_5 + Ccr_2N_2N_5 \quad (2\text{-}13)$$

$$dP_p(z, \lambda)/ dz = [\sigma_{32}(\lambda) N_3 + \sigma_{21}(\lambda) N_2 - \sigma_{13}(\lambda) N_1 - \alpha_p] P_p(z, \lambda) \quad (2\text{-}14)$$

$$dP_s(z, \lambda)/ dz = [\sigma_{54}(\lambda) N_5 - \sigma_{45}(\lambda) N_4 - \alpha_s] P_s(z, \lambda) \quad (2\text{-}15)$$

Where N_1 ($^4I_{15/2}$), N_2 ($^4I_{11/2}$), N_3 ($^4F_{7/2}$), N_4 ($^2F_{7/2}$) and N_5 ($^2F_{5/2}$) are the population densities of relevant energy levels of Er^{3+} and Yb^{3+}. A_{ij} (i, j = 1∼5) is the spontaneous transition rate and non-radiation transition rate between the energy levels i and j. $\sigma_{ij}(\lambda)$ (i, j = 1∼5) is the absorption and emission cross section of the transition between the energy levels i and j.

$P_p(z, \lambda)$ and $P_s(z, \lambda)$ are the corresponding input solar power and output light power, where z is the thickness of the ion doping layer. α_p and α_s are scattering losses and are assumed as frequency-independent constants for the seek of

simplifying the analysis. The concentration-dependent Ccr_1 and Ccr_2 are the ET cross-relaxation co-efficient describing the interaction between Er^{3+} and Yb^{3+}, and they are linearly-increasing functions of the Er^{3+} concentration according to the resonant ET theory.

$$Ccr_1 = 2.0 \times 10^{-21} + 8.00 \times 10^{-48} (N_{Er3+} - 1.0 \times 10^{25}) \qquad (2\text{-}16)$$

$$Ccr_2 = 2.0 \times 10^{-21} + 8.00 \times 10^{-48} (N_{Er3+} - 1.0 \times 10^{25}) \qquad (2\text{-}17)$$

Wij (i, j = 1∼5) is the transition rate between energy levels i and j, and can be expressed as

$$Wi\,j\,(z, \lambda) = \frac{\sigma_{ij}\,(\lambda)\,P\,(z,\lambda)}{h v_{ij} A_{eff}} \qquad (2\text{-}18)$$

Where v_{ij} (i, j = 1∼5) is bandwidth, and A_{eff} is the effective cross-section area. The conservation laws are given by

$$\sum_{i=1}^{3} N_i - N_{Er^{3+}} = 0 \qquad (2\text{-}19)$$

$$\sum_{i=4}^{5} N_i - N_{Yb^{3+}} = 0 \qquad (2\text{-}20)$$

Where N_{Er}^{3+} and N_{Yb}^{3+} are total Er^{3+} and Yb^{3+} concentrations, respectively.

CHAPTER THREE

RESULTS

3.1 Introduction

In this chapter, a promising two-step QC of Er^{3+}-Yb^{3+} codoped fluoride glass will be investigated numerically. Theoretical models of the Er^{3+}-Yb^{3+} system are founded and simulated numerically in order to obtain the power conversion efficiency (PCE) and the quantum conversion efficiency (QCE).

3.2 The Theoretical Model Calculation

We consider an initial steady state. The above model can be solved numerically in python, where the population rate equation groups (2-8)–(2-13) can be solved by Newton's Iterative Method, while the propagation rate equation groups (2-14) and (2-15) form a system of coupled differential equations which can be solved via fourth-order Runge-Kutta methods and some boundary conditions. The modified solar spectrum P_s (z, λ) is optimized and obtained. For simulation, we select fluoride glasses as host materials for spectral downconverters. The spectroscopic parameters used in calculations are chosen carefully from the literature, as listed in Table (3.1).

We choose 489 nm and 923 nm as the Er^{3+} center excitation wavelength and the system Emission wavelength, respectively. Incident solar spectrum is normalized for the case of the complete absorption of incident solar emission in the spectral region corresponding to 489 nm absorption band Of Er^{3+} ions. In order to calculate the effective absorption of input solar spectrum accurately, the Overlap coefficient δ of the Er^{3+} absorption spectrum and the solar spectrum is defined as

$$\delta = \frac{\int_{\lambda} I_{ab}(\lambda) d\lambda}{\int_{\lambda} I_{solar}(\lambda) d\lambda} \qquad (3.1)$$

Table 3.1: Primary parameters in the theoretical model.

Parameter	Symbol	Unit	Value
Scattering loss coefficient	α_p,α_s	db/m	0.1
489nm absorption cross section (Er^{3+})	σ_{13}	m^2	3.7×10^{-21}
923nm radiation cross section (Er^{3+})	σ_{32}	m^2	5.7×10^{-22}
923 nm radiation cross section (Er^{3+})	σ_{21}	m^2	5.7×10^{-21}
Er^{3+} ion spontaneous emission rate	A_{32}	s^{-1}	666.6
Er^{3+} ion spontaneous emission rate	A_{21}	s^{-1}	90
980nm absorption cross section (Yb^{3+})	σ_{45}	m^2	1.32×10^{-24}
980nm radiation cross section (Yb^{3+})	σ_{54}	m^2	1.40×10^{-24}
Yb^{3+} ion spontaneous emission rate	A_{54}	s^{-1}	10

Where $I_{ab}(\lambda)$ and $I_{solar}(\lambda)$ are the Er^{3+} absorption spectrum around 489nm and the solar spectrum around 489 nm, respectively. The calculated δ is 0.371. It means that 37.1% of incident solar energy can be absorbed effectively in the system under 489 nm excitation process. Initial Er^{3+} concentration, Yb^{3+} concentration and the thickness of the spectral downconverter are set to be 1.0×10^{26} ions/m^3, 1.0×10^{26} ions/m^3 and 3 mm, respectively. In order to depict the effect of spectral DC based on 489 nm excitation and 980 nm emission PCE and QCE which are defined as

$$\eta_{PCE} = \frac{\int_{\lambda=200}^{1500} P_s(z,\lambda)d\lambda}{\int_{\lambda=200}^{1500} P_{in}(z,\lambda)d\lambda} \qquad (3\text{-}2)$$

$$\eta_{QCE} = \frac{\int_{\lambda=200}^{1500} N_s(z,\lambda)d\lambda}{\int_{\lambda=200}^{1500} N_{in}(z,\lambda)d\lambda} \qquad (3\text{-}3)$$

The total PCE is defined as the ratio of the total output light power to the total input light power and the total QCE based on the whole solar spectrum in the range of 200 nm-1500 nm is defined as the ratio of the total output photon number to the total input photon numbers.

$$\eta'_{PCE} = \frac{\int_{\lambda=200}^{1500} P_{out}(\lambda,z)\mathrm{d}\lambda}{\int_{\lambda=200}^{1500} P_{in}(\lambda,z)\mathrm{d}\lambda} = \frac{\int_{\lambda=200}^{1500} [P_{in}(\lambda,z)+P_s(\lambda,z)-P_{ab}(\lambda,z)]\mathrm{d}\lambda}{\int_{\lambda=200}^{1500} P_{in}(\lambda,z)} \quad (3\text{-}4)$$

$$q'_{QCE} = \frac{\int_{\lambda=200}^{1500} N_{out}(\lambda,z)\mathrm{d}\lambda}{\int_{\lambda=200}^{1500} N_{in}(\lambda,z)\mathrm{d}\lambda} = \frac{\int_{\lambda=200}^{1500} [N_{in}(\lambda,z)+N_s(\lambda,z)-N_{ab}(\lambda,z)]\mathrm{d}\lambda}{\int_{\lambda=200}^{1500} N_{in}(\lambda,z)} \quad (3\text{-}5)$$

Where $P_{out}(\lambda)$ and $N_{out}(\lambda)$ are the spectrum of total output light power and the spectrum of total output photon number, respectively. $P_{in}(\lambda)$, $P_{ab}(\lambda)$ and $P_s(\lambda)$ are the spectrum of input light power, the spectrum of Er^{3+} absorption power at 489 nm and the spectrum of output light power at 980 nm, respectively. $N_{in}(\lambda)$, $N_{ab}(\lambda)$ and $N_s(\lambda)$ are the corresponding spectrum of the photon numbers.

3.2.1The effect of Er^{3+} - Yb^{3+} concentrations on PCE and QCE

The effect of Er^{3+} and Yb^{3+} concentrations on PCE and QCE is shown in Figure 3.1. Here the thickness of the spectral downconverter is fixed at 3 mm. As Er^{3+} concentration increases from 1.5×10^{26} ions/m^3 to 2.5×10^{26} ions/m^3, PCE and QCE decrease slightly, as shown in Fig. 3.1(A, B).

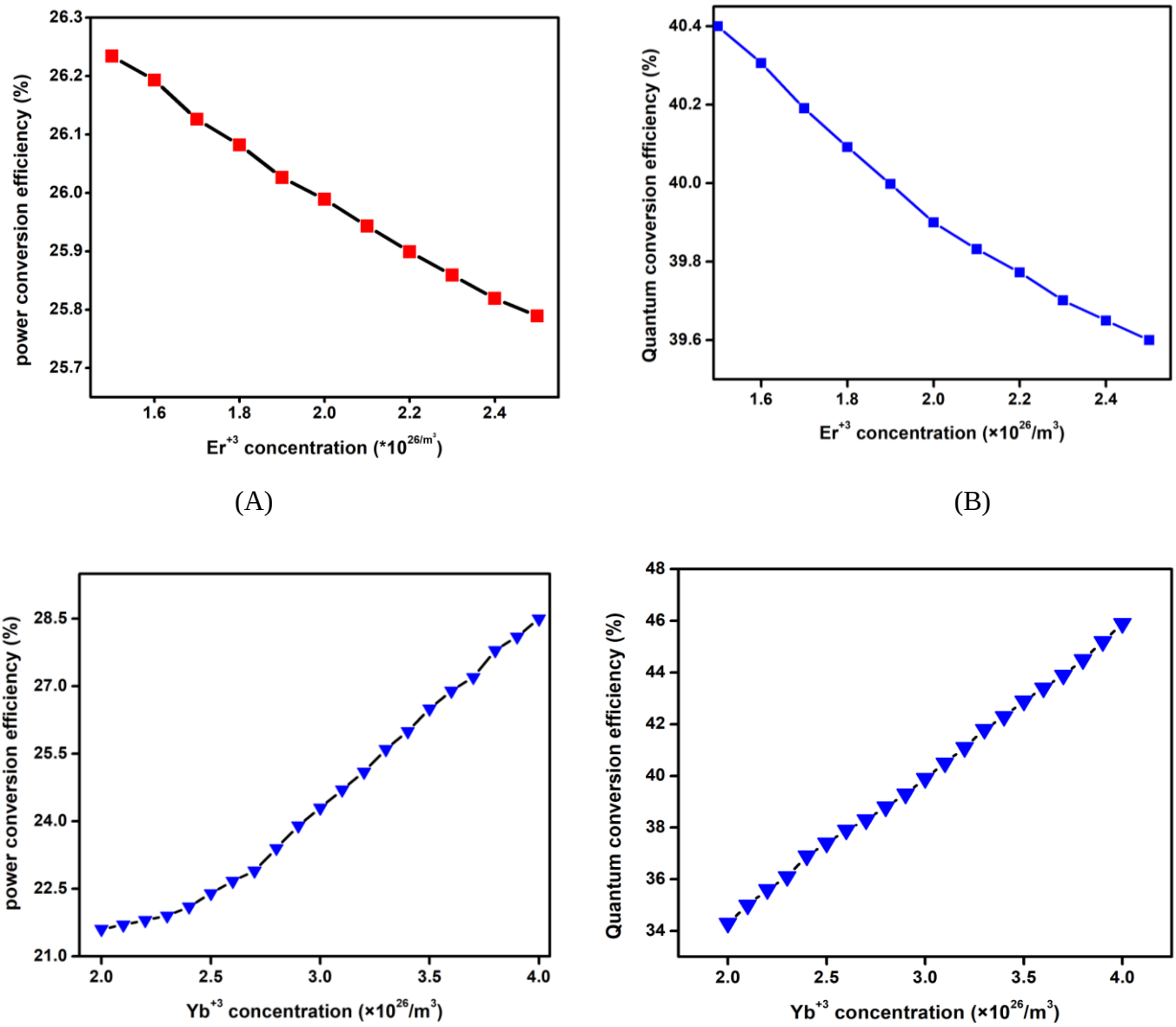

Figure 3.1 Figure 3.2: the thickness of the spectral downconverter .(A) variation of PCE 10^{26} ions/m^3 (B) variation of QCE with × ions/m^3 2.5 × $10^{26}$with Er^{3+} concentration from 1.5 10^{26} ions/m^3 (C) variation of PCE with Yb^{3+}×10^{26}ions/m^3 to 2.5×Er^{3+} concentration from 1.5 concentration from 2.0 ×10^{26} ions/m^3 to 4.0×10^{26} ions/m^3 (D) variation of QCE with Yb^{3+} concentration from 2.0×10^{26}ions/m^3 to 4.0×10^{26} ions/m^3

However, PCE and QCE increases clearly with increased Yb^{3+} concentration from 2.0×10^{26} ions/m^3 to 4.0×10^{26} ions/m^3, as shown in Fig.3.1(C,D).

Figure 3.2indicates that in the definite range of Er^{3+}-Yb^{3+} concentration, the optimal PCE and QCE could be much better for lower Er^{3+} concentration and

higher Yb^{3+} concentration, and moreover, variations of PCE and QCE are less sensitive to a variation of Er^{3+} concentration than to a variation of Yb^{3+} concentration. In our simulation, PCE and QCE reach maximums only when Er^{3+} and Yb^{3+} concentrations reach the optimal values of 1.5×10^{26} ions/m^3 and 2.0×10^{26} ions/m^3, respectively, ascribed to the concentration quenching of Er^{3+} and $Yb^{3+,}$ is observed.

3.2.2 The Effect of the Spectral Downconverter Thickness on PCE and QCE

When investigating the thickness effect of the spectral downconverter on PCE and QCE, both Er^{3+} and Yb^{3+} concentrations are fixed at 1×10^{26} ions/m^3, and Figure 3.2 shows their relationships. As the thickness increases from 1 mm to 10 mm PCE and QCE increase clearly. It should be pointed out that PCE and QCE will no longer increase when the thickness exceeds the maximum (the optimal value), ascribed to absorption losses and side scatting losses within the spectral downconverter [17].

In our simulation, for a thickness of the spectral downconverter z = 3 mm, we obtain the optimal total PCE of 170% and the total QCE of 181% when optimal Er^{3+} and Yb^{3+} concentrations are 1.5×10^{26} ions/m^3 and 4.0×10^{26} ions/m^3, respectively.

We can calculate accurately the efficiency of spectral DC and acquire optimal system parameters: ion concentrations, thickness of the spectral downconverter and NIR QC host materials.

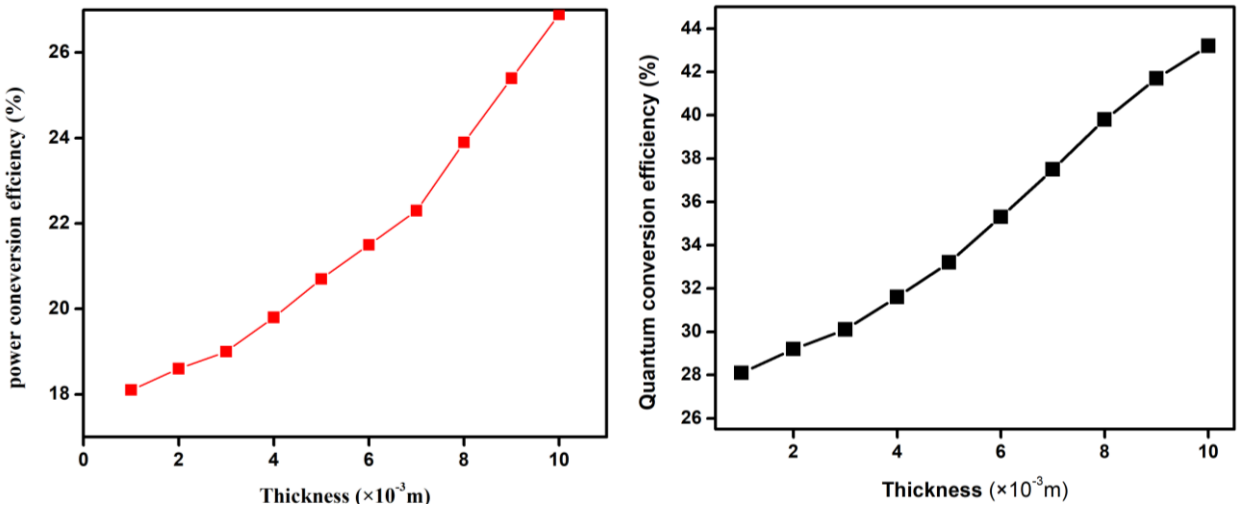

(A) (B)

Figure 3.2: Er^{3+}-Yb^{3+} concentration (A)variation of PCE with the thickness of the spectral downconverter from 1mm to 10 mm (B)variation of QCE with the thickness of the spectral downconverter from 1mm to 10 mm.

CHAPTER FOUR

NUMERICAL RESULT, DISCUSSION AND CONCLUSION

4.1 Discussion

The simulation of rate equation or propagation rate equation resulted in: when the Er^{3+} concentration increases PCE and QCE decrease slightly, while PCE and QCE increases clearly with increased Yb^{3+} concentration and the variation of PCE and QCE with increase the thickness of for Er^{3+}-Yb^{3+} the spectral downconverter resulted in increase the QCE and PCE.

4.2 Conclusions

In conclusion, the ET mechanism of NIR QC for Er^{3+}-Yb^{3+} based on the rate equations and power propagation equations were studied. The NIR QC model is solved numerically in python. Variation of PCE and QCE with the thickness and Er^{3+}-Yb^{3+} concentrations of the spectral downconverter are investigated. In this work, we set up an effective model for simulating Er^{3+}-Yb^{3+} system, and calculate accurately the variation of thickness of PCE and QCE with Er^{3+} and Yb^{3+} and calculate $Er^{3+}$and Yb^{3+} concentration and the variation of PCE and QCE with the thickness of spectral DC and acquire optimal system parameters. The model and technique we propose in this work will be helpful to further investigation and optimization. Much more efficient NIR QC system containing other RE ion couples based on different hosts for further enhancing the ECE of sc-Si solar cells.

REFERENCES

[1] Shockley William Queisser, Hans J., Detailed Balance Limit of Efficiency of p-n Junction Solar Cells , Journal of Applied Physics, 32(1961)510-519

[2]Trupke T, Green MA, Würfel P. Improving solar cell efficiencies by downconversion of high-energy photons. J Appl Phys 2002; 92:1668.

[3] Richards BS, Shalav A. The role of polymers in the luminescence conversion of Sunlight for enhanced solar cell performance. Syn Metals 2005; 154:61.

[4] A. Shalav, Rare-Earth Doped Up-converting Phosphors for an Enhanced Silicon Solar Cell Response, University of New South Wales, PhD Thesis, (2006).

[5] J. Nelson, the Physics of Solar Cell, Imperial College Press, UK, (2003).

[6] Emery, K., Burdick, J., Caiyem, Y., Dunlavy, D., Field, H., Kroposki, B. & Moriarty, T., Photovoltaic Specialists Conference, (1996):1275–1278.

[7] B. M. Van der Ende, L Aarts, A. Meijerink, Phys. Chem. Chem. Phys. 11(2009) 11081-11095.

[8] D. Timmerman, I. Izeddin, P. Stallinga, I. N. Yassievich and T. Gregorkiewicz, Nat. Photonics, 2 (2008) 105-108.

[9] B. Ahrens, Down- and Up-conversion in Fluorozirconate-Based Glasses and Glass Ceramics for Photovoltaic Application, University of Paderborn, PhD Thesis,(2009).

[10] X. Huang, S. Han, W. Huang, X. Liu, Chem. Soc. Rev. 42 (2013) 173-201.

[11] B. Henderson and G. Imbusch, Optical Spectroscopy of Inorganic Solids, Clarendon Press, Oxford, 1989

[12] G. Dieke and H. Crosswhite, the Spectra of the Doubly and Triply Ionized Rare Earths, Journal of Applied Physics, 2, 675 (1963).

[13] R. Wegh, A. Meijerink, R. Lamminmäki, and H. Jorma, Extending Dieke's diagram,, 1002 (2000):87-89.

[14] M. Miritello, L. R. Savio and P. Cardile and F. Priolo, Phys. Rev. B 81 (2010) 041411-041411.

[15] J. Zhou, Y. Teng, G. Lin, J. Qiu, J. Non-Cryst. Solids 357 (2011) 2336-2339.

[16] B. M. Van der Ende, L Aarts, A. Meijerink, Adv. Mater. 21 (2009) 3073-3077.

[17] B. S. Richards, Sol. Energy Mater. Sol. Cells **90**, 2329 (2006).